AD-A154 603 THE IPROP THREE-DIMENSIONAL BEAM PROPAGATION CODE(U) 1/1
MISSION RESEARCH CORP ALBUQUERQUE NM B B GODFREY 1985
AMRC-R-690

UNCLASSIFIED F/G 9/2 NL

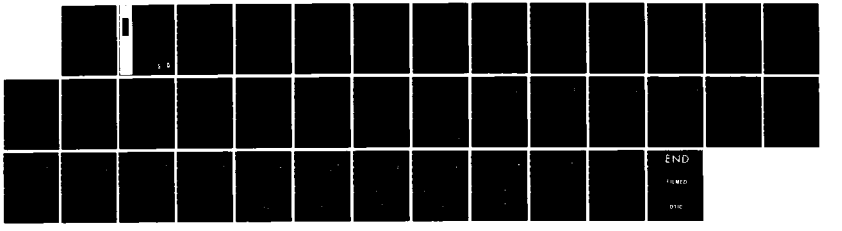

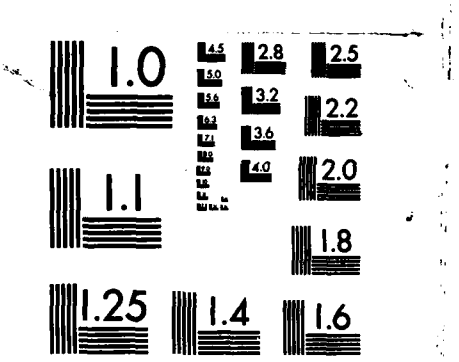

AMRC-R-690
Copy 26

THE IPROP THREE-DIMENSIONAL BEAM PROPAGATION CODE

Brendan B. Godfrey

Presented at: Nonlinear Codes Workshop
Hilton Head Island, South Carolina
11-12 March 1985

Prepared for: Sandia National Laboratories
Pulse Power Directorate
Albuquerque, New Mexico 87185

Work Order: SNL 51-4447

Prepared by: MISSION RESEARCH CORPORATION
1720 Randolph Road, SE
Albuquerque, New Mexico 87106

I. DESIGN PHILOSPHY

IPROP is a nonlinear, three-dimensional, relativistic, electromagnetic particle-in-cell (PIC) beam simulation code written to treat high current electron beam propagation in the atmosphere. As such, it has all the usual features of a plasma simulation code plus air chemistry and particle scattering. The IPROP field solver has been modified to accommodate air conductivity, large aspect ratio spatial zoning, and a moving coordinate mesh. Some specialized diagnostics have been added as well. The field solver, chemistry routine, particle dynamics package, and diagnostics procedures are described in Section II through V, respectively. Here, we comment briefly on the rationale for the particular design chosen for IPROP.

At the time that IPROP was written, in early 1983, the few existing nonaxisymmetric propagation codes were limited to simulating the m=1 hose instability in a single transverse plane.[1-3] Higher azimuthal modes, arising from, for example, filamentation, were not treated. Moreover, the m=1 particle dynamics and air chemistry were linearized. The usual frozen field and paraxial particle motion approximations also were employed.[4] For a variety of reasons these approximations and limitations were incompatible with our needs.

The development of IPROP had been commissioned by Sandia National Laboratories as part of the RADLAC high current beam propagation program. The RADLAC beam was expected to be annular and, therefore, subject to rapid filamentation. VISHNU[5] (and, more recently, IBEX[6]) beam experiments indicated that filamentation typically does not disrupt propagation but can cause the beam radial profile to fill in partially. As a consequence, IPROP had to be capable of following arbitrary azimuthal modes nonlinearly. That the RADLAC beam would rotate required that dynamics in both transverse planes be kept. The frozen field and paraxial particle motion approximations were dropped to permit simulations of near term experiments involving beam energies of a few to several MeV.

It should also be mentioned that the PIC linearized hose codes suffered from noise and numerical instability problems at that time. One significant source of numerical noise is easily identified. Even in the absence of applied forces, perturbed particle positions increase linearly. The effect of this secular growth on the perturbed fields vanishes in the limit of an infinite number of particles, but not uniformly. As time increases in a computation, progressively more particles are required to achieve a given level of cancellation among the secular contributions of the perturbed particles positions to the perturbed currents. Equivalently, for a fixed number of particles the noise level grows with time. This apparently is the cause of the late-time failure of phase-mix damping sometimes observed in such codes. (This difficulty can be overcome by reinitializing perturbed particle quantities every so often, as is done in SIMM1.[3]) Nonlinear simulation codes certainly are not immune to numerical noise. However, years of experience with PIC codes in a variety of applications indicate that noise usually is not a severe problem when reasonable precautions are taken. It may be that nonlinear codes are quieter at late times, because the greatest spatial separation that two particles initially nearby in phase-space can attain is the diameter of a particle orbit.

The occasional exponential growth of perturbed particle orbits in self-pinched equilibria even without perturbed fields, reported in RINGBEARER II simulations,[7] is less easily explained. A simple calculation shows that such behavior is nonphysical. We have speculated that the runaway perturbed positions may be due to stochastic numerical resonance hopping,[8] but we have not pursued this idea. In any event, it did not seem prudent to develop IPROP as a linearized PIC code in the face of this problem of unknown origin.

Practical considerations also influenced the design of IPROP. Earlier, we had written the two-dimensional beam propagation code CPROP,[9] which successfully employed algorithms not involving the frozen field or

paraxial particle approximations. CPROP was developed quickly and at minimal cost from the general purpose two-dimensional plasma simulation code CCUBE.[10] IVORY,[11] the three-dimensional extension of CCUBE, was, therefore, the natural basis for IPROP. Basically, creating IPROP required transferring the CCUBE modifications to IVORY and then devising a method of handling the nonlinear coupling among azimuthal modes of the conductivity and electromagnetic fields. The latter was, of course, not trivial. Upgraded diagnostics were added only recently.

II. THREE-DIMENSIONAL FIELD SOLVER

The CPROP axisymmetric field solver was designed to be numerically accurate and stable for arbitrary scaler conductivities, have an unrestrictive Courant time step limit, allow computations in both the laboratory and beam frames, and accommodate low as well as high energy particle beams. Its nonaxisymmetric generalization is meant, as well, to treat any modestly sized set of not necessarily consecutive azimuthal modes in either or both transverse planes. Following the axisymmetric derivation,[12] we cast Maxwell's equations into coupled forward- and backward-going wave equations.

$$\frac{1}{2}\left[\frac{\partial}{\partial t} + (1 - v)\frac{\partial}{\partial z}\right](E_r + B_\theta) + \frac{1}{2}\left[\frac{\partial}{\partial t} - (1 + v)\frac{\partial}{\partial z}\right](E_r - B_\theta)$$

$$+ \sigma E_r = \frac{1}{r}\frac{\partial}{\partial \theta} B_z - J_r \qquad (1)$$

$$\frac{1}{2}\left[\frac{\partial}{\partial t} + (1 - v)\frac{\partial}{\partial z}\right](E_r + B_\theta) - \frac{1}{2}\left[\frac{\partial}{\partial t} - (1 + v)\frac{\partial}{\partial z}\right](E_r - B_\theta)$$

$$= \frac{\partial}{\partial r} E_z \qquad (2)$$

$$\frac{1}{2}\left[\frac{\partial}{\partial t} + (1 - v)\frac{\partial}{\partial z}\right](E_\theta - B_r) + \frac{1}{2}\left[\frac{\partial}{\partial t} - (1 + v)\frac{\partial}{\partial z}\right](E_\theta + B_r)$$

$$+ \sigma E_\theta = -\frac{\partial}{\partial r} B_z - J_\theta \qquad (3)$$

$$\frac{1}{2}\left[\frac{\partial}{\partial t} + (1 - v)\frac{\partial}{\partial z}\right](E_\theta - B_r) - \frac{1}{2}\left[\frac{\partial}{\partial t} - (1 + v)\frac{\partial}{\partial t}\right](E_\theta + B_r)$$

$$= \frac{1}{r}\frac{\partial}{\partial \theta} E_z \tag{4}$$

$$\frac{1}{2}\left[\frac{\partial}{\partial t} + (1 - v)\frac{\partial}{\partial z}\right] E_z + \frac{1}{2}\left[\frac{\partial}{\partial t} - (1 + v)\frac{\partial}{\partial z}\right] E_z$$

$$+ \sigma E_z = \frac{1}{r}\frac{\partial}{\partial r} r B_\theta - \frac{1}{r}\frac{\partial}{\partial \theta} B_r - J_z \tag{5}$$

$$\frac{1}{2}\left[\frac{\partial}{\partial t} + (1 - v)\frac{\partial}{\partial z}\right] B_z + \frac{1}{2}\left[\frac{\partial}{\partial t} - (1 + v)\frac{\partial}{\partial z}\right] B_z$$

$$= -\frac{1}{r}\frac{\partial}{\partial r} r E_\theta + \frac{1}{r}\frac{\partial}{\partial \theta} E_r \tag{6}$$

The axial mesh velocity v is assumed non-negative for coding convenience.

The six equations are next partially integrated along their axial characteristics and finite differenced axially and radially. We obtain

$$E_r^{n+1,i}\left[\left(\frac{1}{2} + \frac{\Delta t}{2\tau_2}\right) + \frac{\Delta t}{\tau_1}\left(e^{\sigma\tau_1} - 1\right)\right] + B_\theta^{n+1,i}\left(\frac{1}{2} - \frac{\Delta t}{2\tau_2}\right) - \frac{\Delta t}{\tau_1}\left(\frac{e^{\sigma\tau_1} - 1}{\sigma}\right)\frac{1}{r}\frac{\partial}{\partial \theta} B_z^{n+1,i}$$

$$= \frac{\Delta t}{2\tau_2}\left(1 - W_2\right)\left(E_r^{\mu} - B_\theta^{\mu}\right) + \frac{\Delta t}{2\tau_2} W_2 \left(E_r^{n,i+1} - B_\theta^{n,i+1}\right)$$

$$+ \frac{1}{2}\left(1 - W_1\right)\left(E_r^{n,i} + B_\theta^{n,i}\right) + \frac{1}{2} W_1 \left(E_r^{n,i-1} + B_\theta^{n,i-1}\right)$$

$$- \frac{\Delta t}{\tau_1}\left(\frac{e^{\sigma\tau_1} - 1}{\sigma}\right) J_r^{n+1,i} \tag{7}$$

$$E_r^{n+1,i}\left(\frac{1}{2}-\frac{\Delta t}{2\tau_2}\right)+B_\theta^{n+1,i}\left(\frac{1}{2}+\frac{\Delta t}{2\tau_2}\right)-\frac{\partial}{\partial r}E_z^{n+1,i}\,\Delta t$$

$$=-\frac{\Delta t}{2\tau_2}\left(1-W_2\right)\left(E_r^{\mu}-B_\theta^{\mu}\right)-\frac{\Delta t}{2\tau_2}W_2\left(E_r^{n,i+1}-B_\theta^{n,i+1}\right)$$

$$+\frac{1}{2}\left(1-W_1\right)\left(E_r^{n,i}+B_\theta^{n,i}\right)+\frac{1}{2}W_1\left(E_r^{n,i-1}+B_\theta^{n,i-1}\right) \qquad (8)$$

$$E_\theta^{n+1,i}\left[\left(\frac{1}{2}+\frac{\Delta t}{2\tau_2}\right)+\frac{\Delta t}{\tau_1}\left(e^{\sigma\tau_1}-1\right)\right]+B_r^{n+1,i}\left(-\frac{1}{2}+\frac{\Delta t}{2\tau_2}\right)+\frac{\Delta t}{\tau_1}\left(\frac{e^{\sigma\tau_1}-1}{\sigma}\right)\frac{\partial}{\partial r}B_z^{n+1,i}$$

$$=\frac{\Delta t}{2\tau_2}\left(1-W_2\right)\left(E_\theta^{\mu}+B_r^{\mu}\right)+\frac{\Delta t}{2\tau_2}W_2\left(E_\theta^{n,i+1}+B_r^{n,i+1}\right)$$

$$+\frac{1}{2}\left(1-W_1\right)\left(E_\theta^{n,1}-B_r^{n,1}\right)+\frac{1}{2}W_1\left(E_\theta^{n,i-1}-B_r^{n,i-1}\right)$$

$$-\frac{\Delta t}{\tau_1}\left(\frac{e^{\sigma\tau_1}-1}{\sigma}\right)J_\theta^{n+1,i} \qquad (9)$$

$$E_\theta^{n+1,i}\left(\frac{1}{2}-\frac{\Delta t}{2\tau_2}\right)+B_r^{n+1,i}\left(-\frac{1}{2}-\frac{\Delta t}{2\tau_2}\right)-\frac{1}{r}\frac{\partial}{\partial\theta}E_z^{n+1,i}\,\Delta t$$

$$=-\frac{\Delta t}{2\tau_2}\left(1-W_2\right)\left(E_\theta^{\mu}+B_r^{\mu}\right)-\frac{\Delta t}{2\tau_2}W_2\left(E_\theta^{n,i+1}+B_r^{n,i+1}\right)$$

$$+\frac{1}{2}\left(1-W_1\right)\left(E_\theta^{n,i}-B_r^{n,i}\right)+\frac{1}{2}W_1\left(E_\theta^{n,i-1}-B_r^{n,i-1}\right) \qquad (10)$$

$$E_z^{n+1,i}\left[\left(\frac{1}{2}+\frac{\Delta t}{2\tau_2}\right)+\frac{\Delta t}{\tau_1}\left(e^{\sigma\tau_1}-1\right)\right]-\frac{\Delta t}{\tau_1}\left(\frac{e^{\sigma\tau_1}-1}{\sigma}\right)\left(\frac{1}{r}\frac{\partial}{\partial r}r\,B_\theta^{n+1,i}-\frac{1}{r}\frac{\partial}{\partial\theta}B_r^{n+1,i}\right)$$

$$=\frac{\Delta t}{2\tau_2}\left(1-W_2\right)E_z^{\mu}+\frac{\Delta t}{2\tau_2}W_2\,E_z^{n,i+1}$$

$$+\frac{1}{2}\left(1-W_1\right)E_z^{n,i}+\frac{1}{2}W_1\,E_z^{n,i-1}$$

$$-\frac{\Delta t}{\tau_1}\left(\frac{e^{\sigma\tau_1}-1}{\sigma}\right)J_z^{n+1,i} \qquad (11)$$

$$B_z^{n+1,i}\left(\frac{1}{2}+\frac{\Delta t}{2\tau_2}\right)+\frac{1}{r}\frac{\partial}{\partial r}\,r\,E_\theta^{n+1,i}\,\Delta t-\frac{1}{r}\frac{\partial}{\partial\theta}E_r^{n+1,i}\,\Delta t$$

$$=\frac{\Delta t}{2\tau_2}\left(1-W_2\right)B_z^{\mu}+\frac{\Delta t}{2\tau_2}W_2\,B_z^{n,i+1}$$

$$+\frac{1}{2}\left(1-W_1\right)B_z^{n,i}+\frac{1}{2}W_1B_z^{n,i-1} \qquad (12)$$

where

$$\tau_1=\min\left(\frac{\Delta z}{v}\,,\,\Delta t\right)\;;\;\tau_2=\min\left(\frac{\Delta z}{1+v}\,,\,\Delta t\right) \qquad (13)$$

$$W_1=\frac{(1-v)\Delta t}{\Delta z}\;;\;W_2=\min\left(\frac{\Delta z}{(1+v)\Delta t}\,,\,\frac{(1+v)\Delta t}{\Delta z}\right) \qquad (14)$$

and the index pair μ is given by (n+1,i+1) or (n,i) depending on whether W_2 assumes its first or second value in Eq. (13). In the equations Δt is the time step and Δz is the axial cell size. The indices n and i indicate time step and axial cell numbers, respectively, with i increasing from the tail of the beam to the head. See Fig. 1.

Centered radial differences are represented by differentials in Eqs. (7)-(12) for notational simplicity. E_r, B_θ, and B_z are located radially at cell edges, while B_r, E_θ, and E_z are at cell centers. The first three fields are required to vanish on axis. The second three are set to zero at the outer radial edge of the mesh. For simulation of open air propagation, the outer radius is chosen to be at least twenty times the nominal beam Bennett radius. Radial zoning uniform in the coordinate ξ,

$$\xi = a\,\ell n(1+r/a) \qquad (15)$$

with a the Bennett radius, normally is employed to yield cells uniform in size within the beam and expanding linearly at larger radii.

The azimuthal dependences of the field and current components and of functions of the conductivity are given by

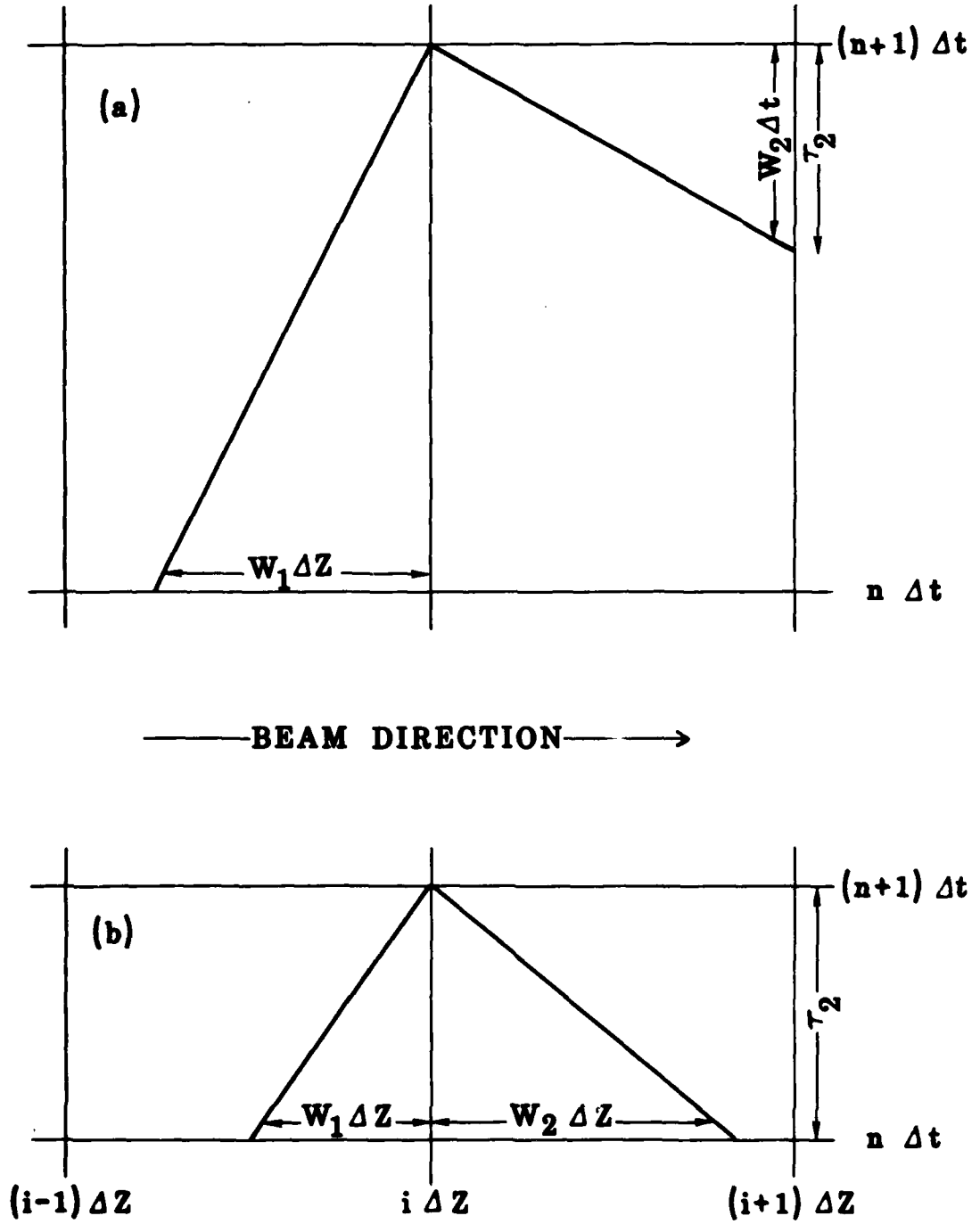

Figure 1. Typical z-t coordinate meshes for (a) $\Delta z < (1+v)\Delta t$, and (b) $\Delta z > (1+v)\Delta t$. Forward- and backward-going light lines, interpolation quantities W_1 and W_2, and forward light line integration time τ_2 also are shown. Omitted are the conductivity characteristic and integration time τ_1.

$$E_z,\ E_r,\ B_\theta,\ J_z,\ J_r,\ f(\sigma) \qquad \begin{cases} \cos m\theta & m > 0 \\ 1 & m = 0 \\ -\sin m\theta & m < 0 \end{cases} \tag{16}$$

$$B_z,\ B_r,\ E_\theta,\ J_\theta \qquad \begin{cases} \sin m & m > 0 \\ 1 & m = 0 \\ \cos m & m < 0 \end{cases} \tag{17}$$

Hence,

$$\frac{\partial}{\partial\theta} \rightarrow m \tag{18}$$

in Eqs. (7)-(12). Consistent with this finite Fourier expansion, products of $f(\sigma)$ and the fields or currents are replaced by convolutions. (Treatment of the convolutions is discussed in the Appendix.) We emphasize that only azimuthal modes of interest need be kept in a particular computation. For instance, simulations of filamentation in the recent IBEX low density air propagation experiments[6,13] might employ only m = 0, 4, 8.

Equations (7)-(12) with auxiliary conditions (13)-(18) are solved numerically at each time step by sweeping axially from the head of the beam back (i. e., decreasing i). At each axial slice the right sides of the equations are evaluated from quantities already known from either the preceding time step or the axial disk next further forward in the beam, as indicated in Fig. 1. E_r and B_r can be eliminated from the left sides of the equations, leaving $4 \cdot N_r \cdot N_\theta$ coupled equations and a like number of unknowns; i.e., of order 10^3 equations and unknowns for typical numbers of radial zones N_r and azimuthal modes N_θ. Although inverting such a system is possible, doing so would be both slow and memory intensive. Instead, azimuthal modes are decoupled by treating the convolutions iteratively, allowing the resulting systems of $4 \cdot N_r$ equations for each mode to be inverted as in CPROP. Beginning with m = 0, we evaluate higher m field contributions to the convolutions using values from the preceding timestep. E_z, B_θ, B_z, and E_θ for m = 0 then are computed from the radial finite difference equations by Gauss elimination, and the corresponding E_r and B_r are determined by back substitution. For the next higher

azimuthal mode, we employ the new field values for m = 0 but the old values for the remaining modes. The radial equations then are inverted just as for m = 0. This procedure is repeated for the remaining azimuthal modes, in each case evaluating the convolutions with the most recent field values available. One may sweep through the modes as often as necessary to obtain the desired accuracy. In practice, we find that a single pass is sufficient. This procedure is straightforward and reasonably fast.

Had the convolutions not been treated iteratively, the Courant condition associated with Eqs. (7)-(12) would be

$$\Delta t < \Delta z/(1-v) \tag{19}$$

Probably, the iteration procedure makes the actual Courant condition more restrictive, but this has caused no apparent difficulties. For v near unity, Δt is constrained by particle dynamics, as in the frozen field approximation.

Fields are initialized at the beginning of a simulation based on the frozen field approximation.

III. AIR CHEMISTRY ROUTINE

IPROP, when first written, employed the PHOENIX air chemistry algorithm developed by Lawrence Livermore National Laboratory.[14]

$$\frac{\partial \sigma}{\partial t} = K \left|J\right| + \nu \sigma - \alpha \sigma^2 \tag{19}$$

In our dimensionless system of units, the impact ionization, avalanche ionization, and recombination coefficients are given by

$$K = 0.593 \tag{20}$$

$$\nu = \frac{1.163 \cdot 10^5 \; P \; S^3}{1 + 2.667 \cdot 10^1 \; S + 2.242 \cdot 10^3 \; S^2 + 6.916 \cdot 10^2 \; S^3} \tag{21}$$

$$\alpha = \frac{3.2 \cdot 10^{-4} P}{(1 + 5.23 \cdot 10^{5} S)^{0.7}} \qquad (22)$$

with $S = (E/P)^2$, the electric field E scaled to 511 kV/cm, and the air density P measured in atmospheres (at standard temperature and pressure).

In the course of delta-ray studies described in Sec. 2.4, we found it useful to replace the constant impact ionization coefficient K in Eq. (20) by a more accurate, energy dependent expression approximating Bethe's electron energy loss formula.[15]

$$K = 0.302 + 0.054 \ln \gamma \qquad (23)$$

where γ is the beam electron average energy, redetermined periodically. (Using the local rather than the average energy would be slightly more accurate but somewhat more expensive computationally.) Equation (23) reduces to Eq. (20) at about 200 MeV. At lower energies the new expression has a slight stabilizing effect on the beam by enhancing impact ionization at the expense of avalanche. For the low current, low energy VISHNU experiments, Eq. (23) was necessary even to obtain correct return current decay times.[8]

Recently, the recombination coefficient α was replaced with

$$\alpha = \frac{1.19 \cdot 10^{-4} P}{(1 + 35.4 S^{1/4} + 44.0 S^{1/2})^{0.39}} \qquad (24)$$

Although we have not yet had the opportunity to assess the effects of this change, it is clear that Eq. (24) leads to faster recombination for larger values of E/P and, therefore, should be stabilizing. At the same time, a temperature dependent momentum transfer cross section was introduced by the simple procedure of multiplying the conductivity by

$$C = \frac{3.02}{(1 + 35.4\ S^{1/4} + 44.0\ S^{1/2})^{0.36}} \tag{25}$$

efore using it in the field solver. Eq. (24) and (25) have been cali-rated against the HICHEM code at high air densities for a wide range of eam currents.

The air conductivity is computed at half-integer timesteps so that it an be advanced with the fields in a leap-frog fashion. The computation is lone in real space to avoid convolutions and then decomposed into azimuthal nodes for use in the field solver. The finite difference equation corres-ponding to Eq. (19) is

$$\sigma^{n+1,i} = \frac{\sigma^o\left[1 + \frac{R+\nu}{2R}\left(e^{R\tau_1}-1\right)\right] + |J|\,\frac{K}{R}\left(e^{R\tau_1}-1\right)}{1 + \frac{R-\nu}{2R}\left(e^{R\tau_1}-1\right) + \sigma^o\,\frac{\alpha}{R}\left(e^{R\tau_1}-1\right)} \tag{26}$$

$$\sigma^o = \left(1 - W_3\right)\sigma^{\mu} + W_3\,\sigma^{n,i+1} \tag{27}$$

$$R^2 \equiv \nu^2 + 4\,\alpha\,K\,|J| \tag{28}$$

with τ_1 defined in Eq. (13) and

$$W_3 = \min\left(\frac{\Delta z}{v\Delta t}\,,\ \frac{v\Delta t}{\Delta z}\right) \tag{29}$$

. . (27), the index pair μ is given by (n+1,i+1) or (n,i) depending on whet.. W_3 assumes its first or second value. Note that Eq. (26) is exact for constant fields.

IV. PARTICLE DYNAMICS

The basic particle transport algorithms are essentially identical to those used in IVORY[11] and so will not be discussed here. Bilinear interpolation is employed in the particle-field interface.

RADIAL DIFFERENCES HANDLED IN STRAIGHTFORWARD MANNER

- RADIAL ZONING UNIFORM IN $\xi = A\ln(1+R/A)$
  NOMINAL BENNETT RADIUS - A
- GIVES SMALL CELLS IN BEAM, LINEARLY EXPANDING CELLS OUTSIDE
- B_z, B_θ, E_r LOCATED AT CELL EDGES, VANISH ON AXIS
- E_z, E_θ, B_r LOCATED AT CELL CENTERS, VANISH AT OUTER RADIAL BOUNDARY - AT LEAST 20 A FOR OPEN AIR

MRC
VG-0510

PARTICULAR FORM OF CONDUCTIVITY INTEGRATING FACTOR CHOSEN TO REPRODUCE CORRECT RESISTIVE DECAY RATES

- $$E_r^{n+1,i}\left[\left(\frac{1}{2}+\frac{\Delta t}{2\tau_2}\right)+\frac{\Delta t}{\tau_1}\left(e^{\sigma\tau_1}-1\right)\right]+B_\theta^{n+1,i}\left(\frac{1}{2}-\frac{\Delta t}{2\tau_2}\right)$$

$$-\frac{\Delta t}{\tau_1}\left(\frac{e^{\sigma\tau_1}-1}{\sigma}\right)\frac{1}{r}\frac{\partial}{\partial\theta}B_z^{n+1,i}=\frac{\Delta t}{2\tau_2}\left(1-W_2\right)\left(E_r^{\mu}-B_\theta^{\mu}\right)$$

$$+\frac{\Delta t}{2\tau_2}W_2\left(E_r^{n,i+1}-B_\theta^{n,i+1}\right)+\frac{1}{2}\left(1-W_1\right)\left(E_r^{n,i}+B_\theta^{n,i}\right)$$

$$+\frac{1}{2}W_1\left(E_r^{n,i-1}+B_\theta^{n,i-1}\right)-\frac{\Delta t}{\tau_1}\left(\frac{e^{\sigma\tau_1}-1}{\sigma}\right)J_r^{n+1,i}$$

- ETC, - SEE PRECEDING FIGURE FOR W, τ, μ DEFINITIONS

MRC
VG-0510

TEMPORAL, AXIAL FINITE DIFFERENCES OBTAINED BY INTEGRATING ALONG CHARACTERISTICS

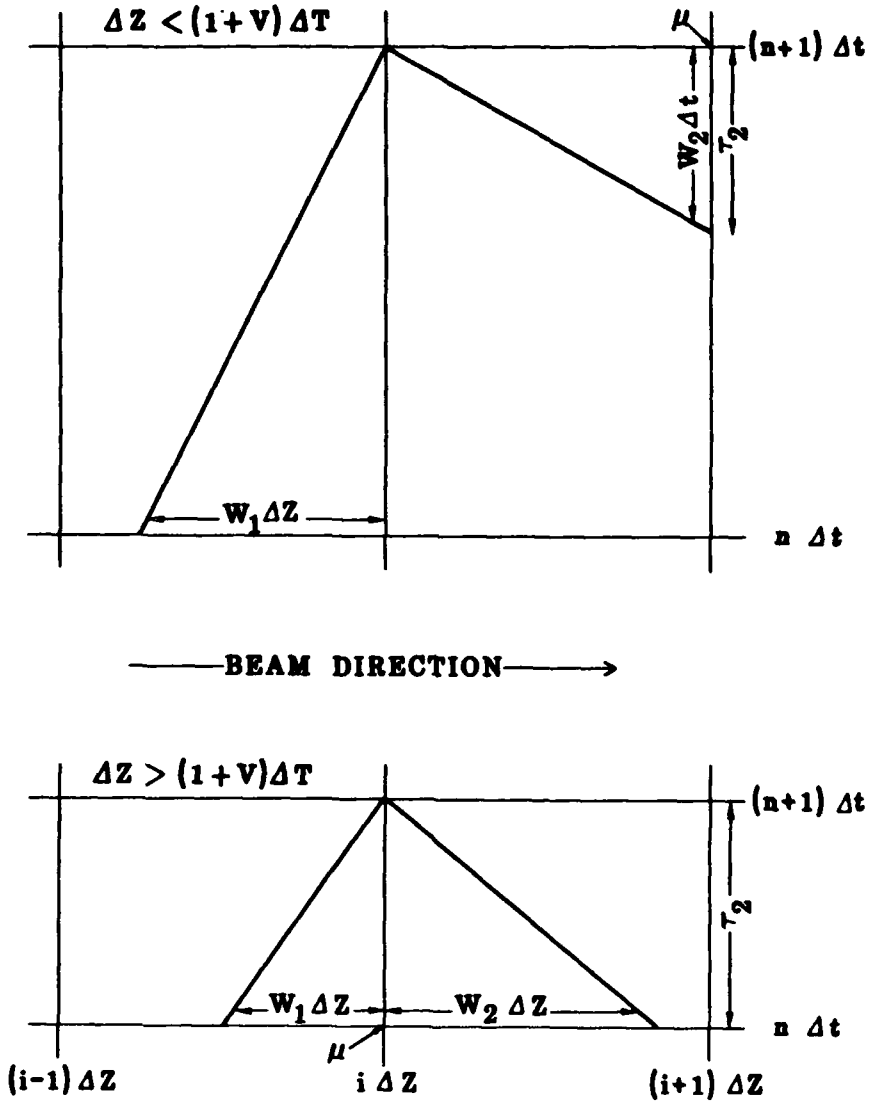

MRC

VG-0510

FIELD ALGORITHM DERIVED FROM MAXWELLS'S EQUATIONS CAST IN TERMS OF FORWARD, BACKWARD GOING WAVES

- $\frac{1}{2}\left[\frac{\partial}{\partial t}+(1-v)\frac{\partial}{\partial z}\right](E_r+B_\theta)+\frac{1}{2}\left[\frac{\partial}{\partial t}-(1+v)\frac{\partial}{\partial z}\right](E_r-B_\theta)$

  $+\sigma E_r = \frac{1}{2}\frac{\partial}{\partial \theta}B_z - J_r$

- $\frac{1}{2}\left[\frac{\partial}{\partial t}+(1-v)\frac{\partial}{\partial z}\right](E_r+B_\theta)-\frac{1}{2}\left[\frac{\partial}{\partial t}-(1+v)\frac{\partial}{\partial z}\right](E_r-B_\theta)$

  $=\frac{\partial}{\partial r}E_z$

- $\frac{1}{2}\left[\frac{\partial}{\partial t}+(1-v)\frac{\partial}{\partial z}\right]E_z+\frac{1}{2}\left[\frac{\partial}{\partial t}-(1+v)\frac{\partial}{\partial z}\right]E_z$

  $+\sigma E_z = \frac{1}{r}\frac{\partial}{\partial r}r\,B_\theta-\frac{1}{r}\frac{\partial}{\partial \theta}B_r - J_z$

- ETC. - MESH VELOCITY IS V

MRC

VG-0510

AZIMUTHALLY VARYING FIELDS TREATED FLEXIBLY BY COMBINATION OF FOURIER, REAL SPACE ALGORITHMS

- PARTICLES TRANSPORTED IN THREE-DIMENSIONAL CARTESIAN GEOMETRY
- FIELDS, CURRENTS COMPUTED IN CYLINDRICAL GEOMETRY, FOURIER DECOMPOSED IN ANGLE
- AIR CONDUCTIVITY EVALUATED IN CYLINDRICAL GEOMETRY, SPATIALLY GRIDDED IN ANGLE
- PARTICLES, FIELDS INTERFACED BY FOURIER TRANSFORM AT EACH PARTICLE LOCATION
- FIELDS, CONDUCTIVITY INTERFACED BY FOURIER CONVOLUTION

MRC

VG-0510

IPROP DESIGNED TO SIMULATE WEAKLY NONLINEAR, COUPLED HOSE AND FILAMENTATION INSTABILITIES

- COMPLETE PARTICLE, FIELD DYNAMICS ACCOMMODATE LOW ENERGY AND ROTATING BEAMS
- FULLY NONLINEAR (STRONG NONLINEARITY REQUIRES MANY MODES)
- TREATS ARBITRARY AZIMUTHAL MODES SEPARATELY OR TOGETHER
- SELECTABLE, VARIABLE MESH VELOCITY PERMITS LABORATORY, BEAM FRAME COMPUTATIONS
- PARTIALLY IMPLICIT FIELD SOLVER, ORBIT AVERAGING RELAX COURANT CONDITIONS
- USES MOLIERE SCATTERING, SAIC E/P CHEMISTRY MODEL

MRC

VG-0510

NONLINEAR CODES WORKSHOP
11 - 12 MARCH 1985

IPROP ALGORITHMS AND CAPABILITIES

BRENDAN B. GODFREY

MRC
mission research corporation

VG-0510

REFERENCES (continued)

15. H. A. Bethe, Z. Physik 76, 293 (1932).

16. W. H. Bennett, Phys. Rev. 45, 890 (1933).

17. W. H. Bennett, Phys. Rev. 98, 1584 (1955).

18. G. Moliere, Z. Naturforsch A3, 78 (1948).

19. E. J. Williams, Proc. R. Soc. London Ser. A 169, 531 (1939).

20. H. A. Bethe, Phys. Rev. 89, 1256 (1953).

21. B. Rossi and K. Greisen, Rev. Mod. Phys. 13, 240 (1941).

22. T. P. Hughes and B. B. Godfrey, Phys. Fluids 27, 1531 (1984).

23. R. R. Johnston, R. L. Feinstein, D. A. Keeley, B. B. Godfrey, L. A. Wright, D. Mitrovich, and T. P. Hughes, "Studies in Charged Particle Beam Propagation (U)," Vol. I, Sec. 3.3 (Science Applications, Int. Corp., Los Altos, 1985) (S/NSI).

24. F. B. Hildebrand, Methods of Applied Mathematics (Prentice Hall, Englewood Cliffs, 1965), Ch. 1.

REFERENCES

1. K. A. Brueckner, "Beam Propagation and Stability (U)," LJI-R-80-061 (La Jolla Institute, San Diego, 1980) (S/NSI).

2. F. W. Chambers, J. A. Masamitsu, and E. P. Lee, "Mathematical Models and Illustrative Results for the RINGBEARER II Monopole/Dipole Beam Propagation Code," UCID-19494 (Lawrence Livermore National Laboratory, Livermore, 1982).

3. G. Joyce and M. Lampe, "SIMM1 - A Linearized Particle Code," NRL 5488 (Naval Research Laboratory, Washington, 1984).

4. E. P. Lee, "The New Field Equations," UCID-17286 (Lawrence Livermore National Laboratory, Livermore, 1976).

5. B. B. Godfrey, R. J. Adler, M. M. Campbell, N. J. Carron, T. P. Hughes, G. F. Kiuttu, N. F. Roderick, and L. A. Wright, "Presentation to DARPA/Services Propagation Review," AMRC-N-232 (Mission Research Corporation, Albuquerque, 1983).

6. DARPA/Services Annual Propagation Review, Proceedings, CONF-8406133 (Lawrence Livermore National Laboratory, Livermore, 1984) (S/NSI).

7. F. W. Chambers, private communication (1983).

8. R. R. Johnston, D. A. Keeley, C. L. Yee, B. B. Godfrey, L. A. Wright, T. P. Hughes, and N. J. Carron, "Charged Particle Beam Propagation Studies," SAI-C-57-PA (Science Applications Inc., Palo Alto, 1983) (S/NSI).

9. B. B. Godfrey, "High Current Beam Propagation Study," AMRC-R-367 (Mission Research Corporation, Albuquerque, 1982).

10. M. M. Campbell, D. J. Sullivan, and B. B. Godfrey, "CCUBE User's Manual," AMRC-R-341 (Mission Research Corporation, Albuquerque, 1982).

11. M. M. Campbell, B. B. Godfrey, and D. J. Sullivan, "IVORY User's Manual," AMRC-R-454 (Mission Research Corporation, Albuquerque, 1983).

12. B. B. Godfrey, in Proc. Tenth Conf. Numerical Simulation of Plasmas, paper 1C6 (San Diego, 1983).

13. C. A. Ekdahl, J. R. Freeman, G. T. Leifeste, R. B. Miller, W. B. Styger, and B. B. Godfrey, submitted to Phys. Rev. Lett. (1985).

14. F. W. Chambers and D. M. Cox, "Standard Test Case Runs for the EMPULSE Monopole Field Solver and Conductivity Generation Model," UCID-19213 (Lawrence Livermore National Laboratory, Livermore, 1981).

ACKNOWLEDGEMENTS

We are endebted to R. B. Miller for encouraging the development of IPROP and to R. L. Feinstein for providing improvements to the air chemistry algorithm.

This research was supported primarily by the Sandia National Laboratories, Albuquerque, with additional funds from the Defense Advanced Research Projects Agency (monitored by the Naval Surface Weapons Center, White Oak). The report itelf is largely extracted from Ref. 23.

$$(Q^T \cdot F \cdot Q)\ (Q^T \cdot E) \tag{A-5}$$

Hence, multiplying the transformed fields by the conductivity tensor $Q^T \cdot F \cdot Q$ generates the desired convolution. Note that, although this discussion is framed in terms of a spatial mesh, the mesh is not actually required for most of the manipulations.

Examples of similarity transformation matrices are

$$Q = \frac{1}{\sqrt{2}} \begin{pmatrix} 1 & 1 \\ 1 & -1 \end{pmatrix}; \quad M = 2 \tag{A-6}$$

$$Q = \frac{1}{\sqrt{3}} \begin{pmatrix} 1 & \sqrt{2} & 0 \\ 1 & \frac{1}{\sqrt{2}} & \sqrt{\frac{3}{2}} \\ 1 & \frac{1}{\sqrt{2}} & -\sqrt{\frac{3}{2}} \end{pmatrix}; \quad M = 3 \tag{A-7}$$

APPENDIX

The azimuthal finite Fourier expansions and resulting convolutions associated with Eq. (16)-(18) are treated explicitly as follows. Suppose that the electromagnetic fields E and B, and the currents J are defined on a uniformly spaced azimuthal mesh of M cells. The fields satisfy differential equations containing the operator

$$D \equiv \frac{\partial^2}{\partial\theta^2} \tag{A-1}$$

The finite difference representation of (A-1) can be diagonalized by means of a similarity transformation on its eigenvectors,[24] evaluated on the mesh and normalized.

$$Q_{n,m} = \psi_m^{(n)} / |\psi_m| \tag{A-2}$$

The unnormalized eigenvectors are

$$\psi_m^{(n)} = \begin{cases} \cos\ (n-1)\ m\Delta\theta & m > 0 \\ 1 & m = 0 \\ -\sin\ (n-1)\ m\Delta\theta & m < 0 \end{cases} \tag{A-3}$$

Here, $\Delta\theta = \theta_{max}/M$. Applying the transformation to D•E yields

$$(Q^T \cdot D \cdot Q)\ (Q^T \cdot E) = \langle -m^2 \rangle\ (Q^T \cdot E) \tag{A-4}$$

where $Q^T \cdot E$ is the transformed field and $\langle -m^2 \rangle$ is a diagonal matrix with elements $-m^2$.

Products of the form $f(\sigma) \cdot E$, appearing in Eq. (7), (9), and (11) are handled in an analogous fashion. Let F be a diagonal matrix consisting of $f(\sigma)$ evaluated at the M azimuthal mesh points. Employing the similarity transformation described above to F•E gives

including comparisons with experiment, has been described in greater detail elsewhere.[22] Scattering is implemented in IPROP by applying a deflection to the beam electrons every few cm of propagation in full density air and proportionately less often at lower densities. The deflection angle is chosen randomly from a large set of previously computed small angles forming a truncated Moliere distribution or from an analytical expression for occasional large angles.

V. DIAGNOSTICS

Satisfactorily displaying three-dimensional phenomena in two-dimensional plots is intrinsically difficult. IPROP diagnostics are for the most part simple generalizations of CPROP diagnostics. Improved output is a subject of continuing research.

Detailed particle behavior is depicted by various two-dimensional projections in six-dimensional phase space. Energy and momentum histograms and time histories of average momenta also are provided. Individual azimuthal modes of the electromagnetic fields and of the beam current, net current, and conductivity distributions are displayed in contour and cross section plots. Time histories of all these quantities at specified locations on the computational mesh are available together with their Fourier spectra. The amplitude and position of the electric field spike also are traced in time. Various radial moments of the beam and net current have been added recently. Other recent additions to the diagnostics are described in Ref. 23.

Output usually takes the form of microfiche and 16 mm color movies. Paper plots and 35 mm color slides also are available.

Several hundred beam electrons are loaded into each axial slice of the coordinate mesh during initialization to give a Bennett radial profile[16,17]

$$J_z = \frac{I}{\pi a^2}\left(1 + \frac{r^2}{a^2}\right)^{-2} \tag{30}$$

with an axially dependent half-radius a. Electron axial momenta are picked from the corresponding relativistically invariant distribution

$$f(p_z) = \frac{1}{T}\,\frac{e^{p_z/T}}{e^{p_o/T} - 1} \qquad p_o > p_z > 0 \tag{31}$$

Specifying the beam energy then determines the transverse momenta. It is easy to show for high energy beams that the resulting transverse momentum distribution is approximately Maxwellian with the RMS average $(p_o T)^{1/2}$. The mechanics of randomly selecting momenta for Eq. (31) is simplified by the usual trick of equating $f(p_z)\,dp_z$ to $d\zeta$, where ζ is a set of random numbers uniformly distributed between zero and one. There results

$$p_z = T\,\ell n\left[1 + \zeta\left(e^{p_o/T} - 1\right)\right] \tag{32}$$

Electrons can be loaded pairwise to minimize statistical fluctuations at early times. The electrons of each pair are separated azimuthally by π but otherwise have identical phase space coordinates.

Electron scattering by air molecules is modeled using the Moliere formalism,[18] which consists basically of Williams scattering[19] at small angles and Coulomb scattering at large.[20] As compared with the usual Rossi-Greisen formalism,[21] Moliere scattering leads to a smaller radial expansion rate combined with a very slow loss of beam particles. The impact of various scattering models on computed Nordsieck lengths,

FIELD EXPANDED AZIMUTHALLY IN SINES, COSINES

- USE SIMILARITY TRANSFORMATION BETWEEN REAL, TRANSFORM SPACES

  $\Rightarrow Q_{n,m} = \psi_m^{(n)} / |\psi_m^{(n)}|$

  $$\Rightarrow \psi_m^{(n)} = \begin{cases} \cos\,(n-1)\; m\Delta\theta & m > 0 \\ 1 & m = 0 \\ -\sin\,(n-1)\; m\Delta\theta & m < 0 \end{cases}$$

- FOURIER TRANSFORMATION OF FIELDS, CURRENTS

  $\Rightarrow E(\omega) = Q^T : E(\theta)$

- FOURIER CONVOLUTION OF CONDUCTIVITY INTEGRATING FACTORS

  $\Rightarrow F(\omega) * E(\omega) = [Q^T : F(\theta) : Q] : [Q^T : E(\theta)]$

MRC
VG-0510

FIELD EQUATIONS INVERTED BY COMBINATION OF EXPLICIT, ITERATIVE, AND IMPLICIT METHODS

- EQUATIONS SOLVED DISK BY DISK FROM HEAD OF BEAM BACK USING DATA FROM EARLIER TIME AND PRECEDING DISK
- AZIMUTHALLY COUPLED MODES (DUE TO CONVOLUTIONS) TREATED ITERATIVELY - USUALLY ONE PASS SUFFICIENT
- RADIAL EQUATIONS FOR EACH AZIMUTHAL MODE TAKE FORM OF FIVE-DIAGONAL MATRIX, SOLVED BY GAUSS ELIMINATION
- RESULTING COURANT CONDITION ON FIELDS NOT RESTRICTIVE

  $\Rightarrow \Delta T < \Delta Z / (1-V)$

MRC

VG-0510

IPROP EMPLOYES E/P AIR CONDUCTIVITY MODEL

- $\sigma = C\ N_e \qquad \frac{\partial N_e}{\partial t} = K\ |J| + \nu N_e - N_e^2$
- BETHE IMPACT IONIZATION COEFFIECIENT (APPROXIMATION)
  - $K = 0.302 + 0.054\ \ell n\ \gamma$
- LLNL AVALANCHE IONIZATION COEFFICIENT (EXPERIMENTAL FIT)
  - $\nu = \dfrac{1.163 \times 10^5\ P\ S^3}{1 + 2.667 \times 10^1\ S + 2.242 \times 10^3\ S^2 + 6.916 \times 10^2\ S^3}$
- SAIC RECOMBINATION COEFFICIENT (FIT TO CODE RESULTS)
  - $\alpha = \dfrac{1.19 \times 10^{-4}\ P}{(1 + 35.4\ S^{1/4} + 44.0\ S^{1/2})^{0.39}}$
- SAIC NORMALIZED MOMENTUM TRANSFER CROSSECTION
  - $C = \dfrac{3.02}{(1 + 35.4\ S^{1/4} + 44.0\ S^{1/2})^{0.36}}$
- $S = (E/P)^2$; P IS NORMALIZED AIR DENSITY

MRC

VG-0510

AIR CHEMISTRY NUMERICAL ALGORITHM EXACTLY SATISFIES MODEL EQUATION FOR CONSTANT SOURCES.

- $$\sigma^{n+1,i} = \frac{\sigma^{o}\left[1+\frac{R+\nu}{2R}\left(e^{R\tau_1}-1\right)\right]+|J|\frac{K}{R}\left(e^{R\tau_1}-1\right)}{1+\frac{R-\nu}{2R}\left(e^{R\tau_1}-1\right)+\sigma^{o}\ \frac{\alpha}{R}\left(e^{R\tau_1}-1\right)}$$

- $$\sigma^{o} = \left(1-W_3\right)\sigma^{\mu}+W_3\ \sigma^{n,i+1}$$

- $$R^2 \equiv \nu^2+4\alpha\ K\ |J|$$

- CONDUCTIVITY, FIELDS EVALUATED ALTERNATELY IN TIME

MRC
VG-0510

PARTICLE EQUATIONS SOLVED WITHOUT LIMITING APPROXIMATIONS

- PARTICLE TRANSPORT IN THREE-DIMENSIONAL CARTESIAN CORDINATES
- Z - R BILINEAR INTERPOLATION OF FIELDS, CURRENTS
- AZIMUTHAL EXPANSION OF FIELDS, CURRENTS AT EACH PARTICLE LOCATION WITHOUT RECOURSE TO INTERMEDIATE MESH
- MOLIERE PARTICLE SCATTERING
- OPTIONAL DELTA-RAY CREATION, TRANSPORT, DEPOSITION

MRC
VG-0510

ORBIT AVERAGING DAMPS NUMERICAL FLUCTUATIONS, REDUCES COMPUTER COSTS

- FIELDS COMPUTED ONLY EVERY N^{th} PARTICLE TIME-STEP
- CURRENT ACCUMULATION OVER N PARTICLE STEPS CUTS NOISE BY $N^{-1/2}$ ⇨ FEWER PARTICLES NEEDED
- ORBIT AVERAGING DEMONSTRATED IN LONG DISTANCE NOSE EROSION SIMULATIONS
- CARE REQUIRED TO AVOID DAMPING PHYSICAL INSTABILITIES
- HIGHER ORDER AVERAGING ALGORITHMS MAY PRESERVE NOISE, COST REDUCTIONS BUT NOT SUPPRESS REAL INSTABILITIES

MRC

VG-0510

COMPREHENSIVE DIAGNOSTICS STILL A SUBJECT OF CONTINUING RESEARCH

- PARTICLE PHASE SPACE TWO-DIMENSIONAL PROJECTIONS
- PARTICLE ENERGY, MOMENTUM HISTOGRAMS
- FIELD, CURRENT, CONDUCTIVITY MODE CONTOURS, CROSSECTIONS
- BEAM, NET CURRENT RADIAL MOMENTS
- VARIOUS TIME HISTORIES, POWER SPECTRA
- MICROFICHE, PAPER, 16 mm COLOR MOVIES, 35 mm COLOR SLIDES

MRC

VG-0510

IPROP VERSATILITY DEMONSTRATED IN DIVERSE APPLICATIONS

- VISHNU BEAM EXTRACTION AND FILAMENTATION SIMULATIONS
- FILAMENTATION SATURATION STUDIES
- PHLAP MULTI-DISK CODE CALIBRATION (IN PROGRESS)
- PHERMEX BEAM HOSE INSTABILITY INTERPRETATION
- IBEX BEAM HOLLOWING-FILAMENTATION COMPARISONS (IN PROGRESS)
- IBEX BEAM HOLLOW HOSE EXPERIMENT INVESTIGATION (IN PROGRESS)

MRC
VG-0510

BEAM TRANSPORT IN IFR CHANNELS ALSO STUDIED WITH IPROP

- CHANNEL ELECTRONS, IONS TREATED AS SECOND, THIRD DISCRETE PARTICLE SPECIES
- AIR CHEMISTRY, PARTICILE SCATTERING NOT USED
- IMPLICIT FIELD SOLVER CRITICAL FOR LARGE PROPAGATION DISTANCES
- PHERMEX, MIMI EXPERIMENT SIMULATIONS SUPPORT ANALYTICAL SCALING LAWS, UNCOVER NEW EFFECTS
- ATA ACCELERATOR TRANSPORT SIMULATIONS POSSIBLE
- CODE ENHANCEMENTS FOR CURVED DRIFTTUBES NEARLY COMPLETED

MRC
VG-0510

SIGNIFICANT IPROP ENHANCEMENTS PLANNED

- INCORPORATE EXISTING ROUTINES FOR MODELING EXPERIMENTAL DIAGNOSTICS
- ADD INTERFACE TO PEGASUS POSTPROCESSOR TO IMPROVE DIAGNOSTICS FLEXIBILITY
- HAND-CODE INNER LOOPS TO DECREASE RUNNING TIME
- PACK FIELD DATA TO REDUCE MEMORY REQUIREMENTS

EXPERIMENTAL PLANNING AND INTERPRETATION TO REMAIN PRIMARY THRUST OF IPROP STUDIES

MRC
VG-0510

ACKNOWLEDGMENTS

- IPROP DEVELOPMENT SUPPORTED BY
  - SANDIA NATIONAL LABORATORIES, ALBUQUERQUE
  - DEFENSE ADVANCED RESEARCH PROJECTS AGENCY (MONITORED BY NAVAL SURFACE WEAPONS CENTER)

- IPROP BASED ON VACUUM TRANSPORT CODE IVORY DEVELOPED FOR LOS ALAMOS NATIONAL LABORATORY
- AIR CHEMISTRY MODEL PROVIDED BY R. L. FEINSTEIN
- CODE OPTIMIZATION, DIAGNOSTICS DESIGN IMPROVED BY M. CAMPBELL, D. GLENN, D. MITROVICH, J. NORTON

MRC

VG-0510

END

FILMED

7-85

DTIC